

Observation of a multiferroic critical end point

Jae Wook Kim¹, S. Y. Haam¹, Y. S. Oh¹, S. Park², S.-W. Cheong², P. A. Sharma³, M. Jain³,
N. Harrison³, Jung Hoon Han⁴, Gun-Sang Jeon¹, P. Coleman², and Kee Hoon Kim¹

¹CSMR & FPRD, Department of Physics and Astronomy,
Seoul National University, Seoul 151-742, South Korea.

²Rutgers Center for Emergent Materials and Department of Physics and Astronomy,
Rutgers University, Piscataway, NJ 08854, USA.

³National High Magnetic Field Laboratory, LANL, Los Alamos, NM 87545, USA.

⁴Department of Physics and BK21 Physics Research Division,
Sungkyunkwan University, Suwon 440-746, South Korea.

The study of abrupt increases in magnetization with magnetic field known as metamagnetic transitions has opened a rich vein of new physics in itinerant electron systems, including the discovery of quantum critical end points with a marked propensity to develop new kinds of order. However, the electric analogue of the metamagnetic critical end point, a "metaelectric" critical end point has not yet been realized. Multiferroic materials wherein magnetism and ferroelectricity are cross-coupled are ideal candidates for the exploration of this novel possibility using magnetic field (H) as a tuning parameter. Herein, we report the discovery of a magnetic-field-induced metaelectric transition in multiferroic BiMn_2O_5 in which the electric polarization (P) switches polarity along with a concomitant Mn spin- \uparrow transition at a critical magnetic field H_c . The simultaneous metaelectric and spin- \uparrow transitions become sharper upon cooling, but remain a continuous crossover even down to 0.5 K. Near the $P = 0$ line realized at $H_c \approx 18$ T below 20 K, the dielectric constant (ϵ) increases significantly over wide field- and temperature (T)-ranges. Furthermore, a characteristic power-law behavior is found in the $P(H)$ and $\epsilon(H)$ curves at $T = 0.66$ K. These findings indicate that a magnetic-field-induced metaelectric critical end point is realized in BiMn_2O_5 near zero temperature.

The term "critical end point" refers to a singular point in the phase diagram of matter at the end of a 1st order phase line, as for example, the liquid-gas critical point of water. The importance of this special point for broad classes of matter has rapidly increased in recent years [1, 2]. Not only can it provide large thermal fluctuations as a necessary ingredient for displaying universal power-law of physical quantities, but in the special case where the phase transition is suppressed to zero temperature, it can give rise to intense quantum mechanical fluctuations with a marked propensity to develop instabilities into new kinds of ground state. The latter case has been recently realized in itinerant metamagnets such as $\text{Sr}_3\text{Ru}_2\text{O}_7$ [3] and URu_2Si_2 [4]. These developments motivate a parallel search for a metaelectric critical end point. By analogy with magnetism, one might expect

such sudden changes in electric polarization to be a rather general phenomenon in (anti)ferroelectric materials under application of an electric field (E). However, to date, those effects have been limitedly observed in specific systems such as relaxor ferroelectrics [5] and DyVO_4 with the Jahn-Teller structural distortion [6]. One possible reason for the scarcity of the phenomenon is the practical difficulty of applying the large voltages required (~ 1 kV) without inducing electrical breakdown. Magnetic fields may in fact be better candidates for inducing metaelectric transitions, for not only do they avoid the problem of electrical breakdown, they provide a reversible method of tuning matter with many well-established advantages over alternative methods such as pressure or chemical doping. This is still a challenging task because of the intrinsically small cross-coupling between spin and lattice degrees of freedom. However, in a special class of matter called multiferroics where the cross-coupling between electricity and magnetism is enhanced, [7, 8, 9, 10, 11, 12], such a rare metaelectric transition, and as its critical end point can be induced by application of magnetic field, as we show in this study.

Among recently discovered multiferroic materials, the family of RMn_2O_5 (R = rare earth, Y) are of particular interest, because of their large dielectric response under magnetic fields [8]. While BiMn_2O_5 is isostructural to RMn_2O_5 (Fig. 1a), its magnetic ground state is distinct from those of other RMn_2O_5 compounds. Only BiMn_2O_5 remains in a commensurate antiferromagnetic (AF) phase below $T_N \approx 40$ K with a propagation vector of $Q = (0.5, 0, 0.5)$ [13, 14], while other RMn_2O_5 compounds develop an instability into an incommensurate (IC) AF structure below $T_{IC} \approx 25$ K [13]. According to DC magnetization (M) (Fig. 2a) and neutron diffraction data [14], BiMn_2O_5 has a typical AF spin ordering with an easy axis almost parallel to the a -axis without showing any signature of a spiral ordering. At T_N , the development of magnetic order is accompanied by the growth of ferroelectric (FE) polarization P and a sharp peak in the dielectric constant ϵ (Figs. 2b and 2c).

Multiferroicity in materials with incommensurate spiral spin ordering is normally accounted for in terms of the "spin-current model" [15]. Recent neutron scattering studies of RMn_2O_5 ($R = \text{Tb}, \text{Ho}, \text{Y}$, and Bi) [14, 16, 17] have suggested an alternative "exchange-striction" sce-

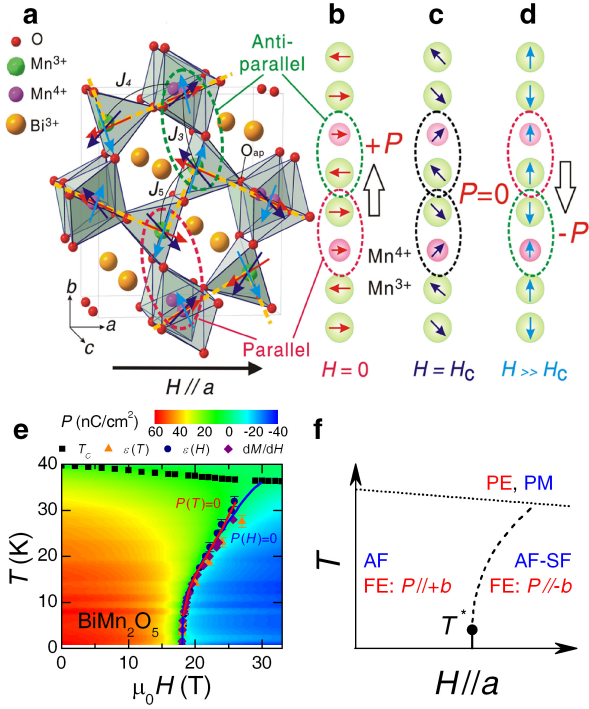


FIG. 1: Magnetic structure and phase diagram. (a) The structure and AF zigzag spin chains under various magnetic fields for BiMn₂O₅. J_3 and J_4 denote the interchain and intrachain exchange interactions between Mn³⁺-Mn⁴⁺ spin pairs, respectively, while J_5 describes that between neighboring Mn³⁺ spins in the bi-pyramid. Red, dark blue, and light blue arrows represent spin directions at $H=0$, $H=H_c$, and $H \gg H_c$, respectively. The corresponding simplified spin arrangements and the net P (black open arrows) are shown for (b) $H=0$, (c) $H=H_c$, and (d) $H \gg H_c$. (e) The H - T phase diagram and the intensity contour of P based on the $P(H)$ data. All symbols were determined from the peak positions of $\chi(H)$, $\chi(T)$, and dM/dH . (f) Suggested schematic phase diagram. Dotted, solid, and dashed lines indicate the 2nd-order paraelectric (PE)-FE transition, 1st-order AF to spin-ordered AF (AF-SF) transition, and AF to AF-SF crossover, respectively. A possible critical end point T^* is denoted as a solid circle.

nario for this commensurate magnetic system. The AF phase of RMn₂O₅ involves zigzag chains of spins (dashed orange lines in Fig. 1a) with a staggered moment lying almost parallel to the Mn³⁺-O_{ap} bond (where O_{ap} is the apical oxygen in each pyramid). Neutron measurements show that the staggered moment is tilted away from the a -axis by about 8° at low temperatures [14], an effect which is presumably driven by a large single-ion anisotropy in the pyramid and strong AF exchange interactions along the chain (i.e., large J_4 and $J_5 > 0$ in Fig. 1a) [16]. The effect of stacking AF zigzag chains along the b -axis leads to a member frustrated Mn spin loop in the ab -plane: Mn⁴⁺-Mn³⁺-Mn³⁺-Mn⁴⁺-

Mn³⁺. Although the nearest-neighbor magnetic coupling in the loop is antiferromagnetic, the odd number of bonds leads to frustration of the spins, preventing them from being antiparallel on every bond in the loop. Due to the relatively small exchange interaction between Mn³⁺-Mn⁴⁺ ions (J_3), the system forms a unique spin ordering pattern [14]: half of the Mn³⁺-Mn⁴⁺ spin pairs across neighboring zigzags are approximately antiparallel, whereas the other half are almost parallel. Under this spin arrangement, exchange-striction between the Mn³⁺-Mn⁴⁺ spin pairs shifts ions (mostly Mn³⁺ inside pyramids) in a way that optimizes the spin-exchange energy: ions with antiparallel spins are pulled towards each other (green dashed circle in Fig. 1a), while those with parallel spins move apart (red dashed circle) [18]. This exchange-striction mechanism then results in canted staggered electric dipoles that are aligned parallel to the Mn³⁺-O_{ap} bond in each bi-pyramid, leading to an electric polarization P along the b -axis (Fig. 1b).

The application of high magnetic fields along the a -axis reveals unexpected magnetic and electric anomalies (Fig. 2); a sharp symmetric peak in the dM/dH curve (Fig. 2e) is accompanied by a sharp increase in $\chi(H)$ and a polarization $P(H)$ which passes through zero (Fig. 2d and 2f). The critical fields for these anomalies increase with temperature, and more or less coincide. Similarly, the temperature of the $\chi(T)$ peaks correspond to the temperature where the polarization $P(T)=0$ (Figs. 2b and 2c). A contour intensity plot of the $P(H)$ curves (Fig. 1e) confirms that the trajectory of the $P(H)=0$ (blue solid line) closely matches that of the $P(T)=0$ (red solid line), and the peak positions of $\chi(H)$, dM/dH , and $\chi(T)$ curves below 20 K.

We attribute the origin of the magnetic anomaly to a spin-ordered (SF) transition in the AF zigzag spin chains. This is supported by an observation of a small M value and a zero-crossing of the linearly extrapolated line at $H > H_c$, indicating the survival of the AF interaction beyond H_c (Fig. 2e, inset). While the SF is often manifested as a 1st-order transition, in this case the $M(H)$ curve does not show a discontinuity down to 0.5 K, as evidenced by a lack of divergence in the dM/dH curve. This characteristic is also observed in the electric properties; the $P(H)$ curve at 0.66 K does not show a discontinuity and the $\chi(H)$ curve does not show divergence even at $T=0.66$ K except sharpening on cooling. Furthermore, the $\chi(H)$ curves measured in very slow H - or T -sweeps did not show any obvious hysteresis (See, a supplementary figure, Fig. S1). The lack of a sharp 1st-order transition feature becomes more evident in the $P(T)$ curves (Fig. 2c), in which P gradually changes its magnitude and sign on cooling. In addition, our preliminary T -dependent specific heat measurements across the $P=0$ line show no peak structure or discontinuity. These observations strongly suggest that the SF transition and concurrent electrical transition occur via a smooth crossover down to temperatures as low as 0.5 K, during which the spin configuration changes continuously

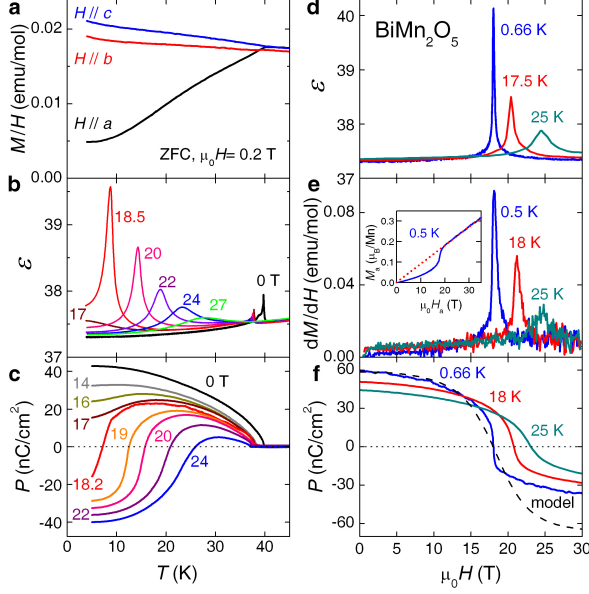


FIG. 2: Electric and magnetic properties of BiMn_2O_5 . (a) M/H measured along the three crystallographic directions. (b) $\epsilon(T)$ data down to 4 K at various magnetic fields. The $\epsilon(H=0)$ peak near 40 K represents the FE transition. (c) $P(T)$ curves at various magnetic fields, showing a crossover from positive to negative. (d) $\epsilon(H)$ at fixed temperatures. (e) Field-dependent dM/dH curves at fixed temperatures. The inset shows the $M(H)$ curve at $T = 0.5$ K. (f) $P(H)$ at fixed temperatures. The dashed line shows the calculated P curve as predicted by the spin-rotation model described in the text and in Fig. 1 (b-d). All dotted lines are guides for the eye.

from the AF- (Fig. 1b) to the SF-type (Fig. 1d).

In fact, continuous spin- \uparrow spin- \downarrow transitions are well known in antiferromagnets when the field H is applied at an angle to the easy axis: typically, a spin- \uparrow spin- \downarrow crossover occurs when the angle between the field and the staggered moment exceeds a certain critical value [19, 20]. This case has been well studied in uniaxial antiferromagnets such as GdAlO_3 [19] and MnF_2 [20]. In the former, the critical angle starts from zero at $T_N = 3.2$ K and grows as the temperature is lowered, reaching 10° at zero temperature. So long as the magnetic field inclination exceeds the critical angle, a cross-over is observed, but when the critical angle reaches the field-inclination angle, the system passes through a critical end point, located at a temperature T_c in the H - T plane and at lower temperatures the SF sharpens into a first order transition. In spin- \uparrow spin- \downarrow transitions, the location of T_c is determined as a function of the initial angle between the spin easy axis and the applied field.

We can easily generalize this understanding to the case of BiMn_2O_5 . Fig. 1a shows that in BiMn_2O_5 , the zig-zag

chain of Mn spins (red arrows) subtend an angle of 8° to the a -axis, providing an intrinsic "tilt" with respect to a field applied along the x axis. In this way, the zig-zag chain provides a natural mechanism for a spin- \uparrow spin- \downarrow crossover down to some critical temperature T_c . This leads us to identify the $P = 0$ trajectory in the phase diagram of BiMn_2O_5 (Fig. 1e) with the spin- \uparrow spin- \downarrow crossover line above $T > T_c$. Our data enable us to estimate the critical temperature T_c is at, or below 0.5 K.

One of key findings of this work is the SF crossover can drive the continuous H -induced P reversal at $T > T_c$ via the exchange-striction mechanism. To understand the mechanism, consider the effect of a magnetic field H on a single AF zigzag chain. If we assume that the interchain coupling (J_3) can be neglected, then the dominant intrachain coupling (J_4 and J_5) will give rise to an almost antiparallel spin alignment. The magnetic free energy of the AF zigzag chain at zero temperature will then be governed by that of a pair of Mn^{3+} spins in the bi-pyramid, consisting of the energies of the AF spin sublattice and the single-ion anisotropy of the Mn^{3+} spins [21]: $F_M = \mu_B \mu_k + (\chi_k - \chi_\perp) \sin^2 \theta \cos^2(\theta - \theta_0)$. Here, χ_k and χ_\perp are magnetic susceptibility values parallel and perpendicular to the staggered moment, respectively. The parameters θ_0 and θ denote the angle between the Mn^{3+} spin direction and the a -axis, the value of θ at zero field and the single-ion anisotropy energy, respectively. The value at each H leading to the minimum energy can be obtained from $\partial F_M / \partial \theta = 0$ and the resultant following relationship:

$$\tan 2\theta = \frac{\tan 2\theta_0}{1 - \frac{(\chi_k - \chi_\perp) H^2}{\cos 2\theta_0}} \quad (1)$$

The above equation predicts that when $\theta_0 > 0$ (< 0), θ increases (decreases) continuously with H to cross the angle 45° (-45°) at $H_c = \frac{\cos 2\theta_0}{\cos 2\theta_0 - (\chi_k - \chi_\perp)}$. In other words, the spin rotation occurs in a way that each AF zigzag chain rotates counter-clockwise or clockwise alternatively to cross 45° or -45° at H_c (dark blue arrows in Fig. 1a). When we consider the special 45° configuration (Fig. 1c), in which the angle between Mn^{3+} and Mn^{4+} spins becomes 90° , the exchange-striction is balanced and gives $P = 0$. On further increasing H , θ increases to make the spin alignment almost perpendicular to the field (blue arrows in Fig. 1a). As a result, the relative orientation of neighboring Mn spins reverses as a function of field (see Fig. 1. b and d) giving rise to the sign reversal in the electric polarization P .

For comparison with the experimental data, we have calculated predicted value of $P/S^{4+}S^{3+} \cos 2\theta$ with determined in Eq. (1). Here, S^{4+} and S^{3+} are the spin vectors of neighboring Mn ions between the AF zigzag chains. The dashed line in Fig. 2f shows the calculated $P(H)$ curve with $\mu_0 H_c = 18.04$ T and $\theta_0 = 8^\circ$, showing a qualitative agreement with the curve at $T = 0.66$ K. Therefore, the rather continuous magnetic field-induced P reversal observed in BiMn_2O_5 can be accounted for by the variation of exchange-striction degree driven by

the Mn spin-*op* crossover. We further note that only BiMn₂O₅ has a homogeneous positive *P* below *T_C* under small electric poling; all the other RMn₂O₅ develop additional FE domains with negative polarity and antiphase domain wall boundaries below *T_{IC}* [22]. In turn, the above *P* reversal model can be applied to BiMn₂O₅ only, and it appears to explain why the experimental finding of *P* reversal as well as "*ε*" increase near *H_c* are unique to BiMn₂O₅ [23].

The magnetically induced polarization reversal we observe is closely analogous to the field-induced metamagnetic transitions observed in spin systems [1, 24] and is most naturally regarded as a magnetic-field induced "metaelectric" transition [6]. As the inversion symmetry is already broken in both sides of the *H_c*(*T*) boundary in Fig. 1f, the metaelectric transition involves only a change in the magnitude of the ferroelectric order parameter *P*. In this case, due to the coupling of *P* to the Mn spin moment, the metaelectric transition occurs as a crossover down to very low temperatures (*T* = 0.5 K). The system-atically increased sharpening observed in "*ε*(*H*)", *dM*=*dH* and *P*(*H*) curves upon cooling all indicate that *T_c* is close to 0.5 K. If so, we would expect to observe critical fluctuations associated with the critical end point, with a power-law evolution of the physical quantities in close proximity to *T_c*. Our experiment confirms this expectation as shown in Figs. 3a and 3b, where ("*ε*(*H*) - *ε*(*H* = 0))⁻¹ vs. *h*^{2/3}" and "*P* vs. *h*^{1/3}" plots produce quite linear behavior. Here *h* = [*H* - *H_c*]/*H_c* is the normalized deviation from the critical field *H_c* = 18.04 T. The linearity observed over a broad range of *h* (*h* = 0.004-0.45 for "*ε*") means that a single power-law of *P* / *h*^{1/3} can robustly explain the experimental data, even for *H* very close to *H_c*. Furthermore, our attempts to fit the data at temperatures above 1.5 K reduce the linearity range for both "*ε*" and *P* vs. *h* so that the power-law becomes most evident at the lowest temperature available, *T* = 0.66 K, in our experiment.

We find that the peculiar power-law of *P* and "*ε*" near *T_c* can be effectively described by a Landau-Ginzburg-type free energy *F* = *F_{ME}* + *F_E*, where

$$F_{ME} = a(S^{4+} - S^{3+})P = a(H - H_c)P \quad (2)$$

and

$$F_E = \frac{b}{2}(T - T_c)^n P^2 + \frac{u}{4}P^4. \quad (3)$$

The magnetoelectric free energy *F_{ME}* consists of a coupling term between the spin orientations and the electric polarization, while the ferroelectric free energy *F_E* effectively describes the evolution of *P* as a crossover at *T* > *T_c* and as a 1st-order transition at *T* < *T_c* under the assumption that the coefficient of *P*² changes its sign across *T_c*. Here, *n* refers to an arbitrary exponent to describe temperature-dependence of physical quantities near *T_c* and *n* = 1 in the classical case. The second-derivative of *F_E* with respect to *P* determines the dielectric susceptibility $\chi^{-1}_e(P) = b(T - T_c)^n + 3uP^2$, where "*ε*" = $\chi_e(P) + 1$.

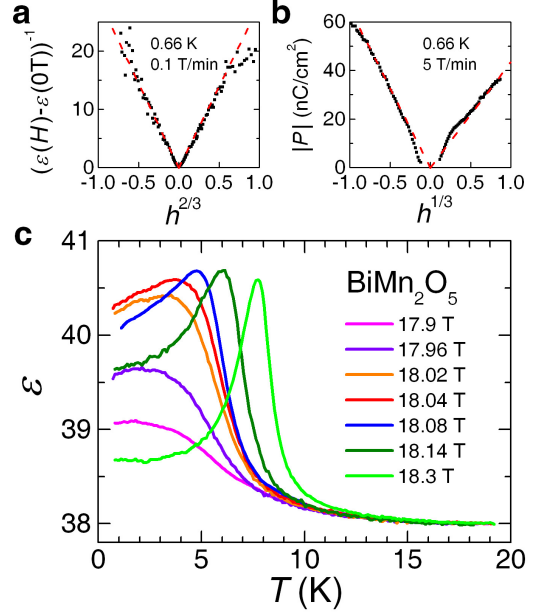


FIG. 3: Field-induced power-law evolution and "*ε*" anomaly at very low temperature. (a) ("*ε*(*H*) - *ε*(*H* = 0))⁻¹ vs. *h*^{2/3}", where *h* = (*H* - *H_c*)/*H_c* and *H_c* = 18.04 T. A very slow ramping rate (0.1 T/min) was used for the "*ε*(*H*)" measurement. The red dashed lines are linear guides passing through the origin. The linear relationship was valid in a wide *h* = 0.004-0.45 (i.e., *H* - *H_c* = 0.1-8 T). (b) Plot of *P* vs. *h*^{1/3}. The linear regime of *h* was *h* = 0.02-0.45 (*H* - *H_c* = 0.3-8 T). To increase the signal-to-noise ratio, it was necessary to choose a rather fast ramping rate (5 T/min) for the *P*(*H*) measurement, which made the *P* data less reliable in a small *h* region. (c) Detailed "*ε*(*T*)" curves down to *T* = 0.6 K at fixed *H* near *H_c*. The shape of the "*ε*(*T*)" curves above the maximum temperature was similar to that predicted by Barrett's theory (Fig. S2).

The sharp increase in ϵ observed in experiments can be understood as the closeness of the system to the critical end point *T_c*. In our Landau-Ginzburg model, when the temperature is approximately *T_c*, the physics is driven by the interplay between the dominant quartic *P*⁴ term and linear *P* term. Under this assumption, $\partial(F_{ME} + F_E)/\partial P|_{P=0} = 0$ provides *P* / (*H* - *H_c*)^{1/3}. Furthermore, $\partial^2(F_{ME} + F_E)/\partial P^2|_{P=0} = 3uP^2 / (H - H_c)^{2/3}$. These predicted exponents are consistent with those determined experimentally (Figs. 3a and 3b), clearly supporting the existence of *T_c* near 0.66 K.

The low value of *T_c* found in our experiments suggests that BiMn₂O₅ lies close to a metaelectric quantum critical point, where *T_c* is actually zero. Closely analogous behavior is well-known in the case of the itinerant magnet Sr₃Ru₂O₇ [1]. In this respect, several novel features of the present data particularly prompt further

notice. First, the observation of the robust power-law of $P/h^{1=3}$ suggests a unique mean-field type while the system is expected to have a 3D Ising universality class ($P/h^{1=4.82}$) near the classical critical end point as seen in the liquid-gas transition. Moreover, the trajectory of the crossover temperature near the zero temperature limit following $(H-H_c)^{1=2}$ (Fig. 1e) again constitutes another mean-field type behavior. Thus, all these observations suggest that the effective dimension of the system has been lifted up to 4 or higher so as not to produce the expected 3D fluctuation. One possible origin for such a dimensional increase is in fact the dynamic exponent effect expected due to the prevailing quantum critical end point fluctuation.

The insights gained by our measurements and analysis above suggest that the multiferroic BiMn_2O_5 provides a rare opportunity to find a multi-ferroic quantum critical point and to test its influence on ferroelectric materials. Supporting this novel conclusion, detailed $\chi(T)$ shape realized near H_c (Fig. 3c) further reveals a clue toward detecting the quantum critical signature. When H approaches 18.04 T from below, systematic increase of $\chi(T=0.66\text{ K})$ occurs. In particular, at $\mu_0 H_c = 18.04\text{ T}$, χ continues to increase as T decreases from 20 K and shows a broad maximum around 4 K, followed by a slight decrease of 0.5 % down to 0.6 K. The behavior qualitatively resembles that of the $\chi(T)$ curve in quantum paraelectric systems, such as SrTiO_3 [25, 26, 27, 28]. Furthermore, the increase in $\chi(T)$ between 4 and 20 K is not proportional to the inverse of temperature, as expected in classical paraelectrics. Instead, it is closer to the shape predicted by Barrett's theory (Fig. S2) [29], indicating that the enhanced lattice fluctuation in close vicinity to T_c is linked to the quantum mechanical population of the relevant phonon mode. Therefore, the physics of BiMn_2O_5 appears to involve quantum zero point lattice motion at low temperatures as does SrTiO_3 . The uniqueness of BiMn_2O_5 lies in the magnetic-field-tunability of its quantum-paraelectric properties.

Our observations raises the interesting possibility that instabilities into new quantum states of matter might develop in close vicinity to the multi-ferroic critical end point, as they do close to the magnetic quantum critical end point in $\text{Sr}_3\text{Ru}_2\text{O}_7$. In future work we plan to investigate this possibility by fine-tuning the T position, either by rotating the field direction or by applying external pressure.

M methods

Single crystal samples were grown using the flux method [8]. All the electrical properties were measured along the b -axis while the magnetic field was applied along the a -axis up to 35 T at the National High Magnetic Field Laboratory (NHMFL). Dielectric constants were measured by a capacitance bridge (GR1615A or AH2500A) at 1 kHz [23]. P was obtained by integration of the pyro- and magnetoelectric currents measured by use of an electrometer (Keithley 617). Given the limited magnet time for high-field measurements, the continuous application of a small electric field bias of $E = 2\text{ kV/cm}$ was quite useful in quickly determining the P evolution. In particular, the value of $E = 2\text{ kV/cm}$ was sufficient to fully polarize the sample on cooling through T_c but small enough to produce a P close to its spontaneous value. In several field and temperature sweeps, it was verified that the spontaneous P measured under zero electric field after poling with $E = 2\text{ kV/cm}$ is close to the P measured under the same bias. A precalibrated capacitance sensor was used for accurate T -sweeps between 0.6 and 20 K near H_c (Fig. 3c), while a Cemox sensor was mostly used for the T - and H -sweeps above 4 K. For H -swept measurements at $T = 0.66\text{ K}$ and 1.5 K , temperatures were stabilized by controlling the vapor pressure. Specific heat and magnetocaloric effects were measured with a plastic calorimeter. Temperature-dependent DC magnetization was measured using a vibrating sample magnetometer in a Physical Property Measurement System (Quantum Design). A pickup-coil magnetometer was used to measure the H -dependent magnetization in a pulse magnet at NHMFL-Los Alamos National Laboratory.

Acknowledgments

We thank P. Chandra, S. Rowley, J. Schmalian, and G. R. Stewart for stimulating discussions. This study was supported by Korean Government through NRL (M10600000238) and GPP programs, and by KRF (KRF-2008-205-C00101). JW was supported by Seoul R&BD. Work at Rutgers was supported by NSF-0405682 and NSF-DMR-0605935. Work at NHMFL was performed under the auspices of the National Science Foundation, the State of Florida, and the U.S. Department of Energy.

[*] Corresponding author: khkim@phys.snu.ac.kr

[1] Grigera SA et al. (2001) Magnetic field-tuned quantum criticality in the metallic ruthenate $\text{Sr}_3\text{Ru}_2\text{O}_7$. *Science* 294:329-332.

[2] Harrison N, Jain M, Mydosh JA (2003) Reentrant hidden order at a metamagnetic quantum critical end point. *Phys Rev Lett* 90:096402.

[3] Grigera SA et al. (2004) Disorder-sensitive phase formation

linked to a metamagnetic quantum criticality. *Science* 306:1154-1157.

[4] Kim KH et al. (2004) Nexus between quantum critically and phase formation in $\text{U}(\text{Ru}_{1-x}\text{Rh}_x)_2\text{Si}_2$. *Phys Rev Lett* 93:206402.

[5] Kutnjak Z, Petzelt J, Blinc R (2006) The giant electromechanical response in ferroelectric relaxors as a critical phenomenon. *Nature*, 441:956-959.

- [6] Vekhter BG, Kaplan MD (1979) A new type of structural Jahn-Teller phase transition in DyVO_4 induced by an electric field. *JETP Lett* 29:155-157.
- [7] Kimura T et al. (2003) Magnetic control of ferroelectric polarization. *Nature* 426:55-58.
- [8] Hur N et al. (2004) Electric polarization reversal and memory in a multiferroic material induced by magnetic fields. *Nature* 429:392-395.
- [9] Spaldin NA, Fiebig M (2005) The renaissance of magnetoelectric multiferroics. *Science* 309:391-392.
- [10] Eerenstein W, Mathur ND, Scott JF (2006) Multiferroic and magnetoelectric materials. *Nature* 442:759-765.
- [11] Tokura Y (2006) Multiferroics as quantum electromagnets. *Science* 312:1481-1482.
- [12] Kenzelmann M et al. (2007) Direct transition from a disordered to a multiferroic phase on a triangular lattice. *Phys Rev Lett* 98:267205.
- [13] Muñoz A et al. (2002) Magnetic structure and properties of BiMn_2O_5 oxide: A neutron diffraction study. *Phys Rev B* 65:144423.
- [14] Vecchini C et al. (2008) Commensurate magnetic structures of RMn_2O_5 ($\text{R} = \text{Y}, \text{Ho}, \text{Bi}$) determined by single-crystal neutron diffraction. *Phys Rev B* 77:134434.
- [15] Katsura H, Nagaosa N, Balatsky AV (2005) Spin current and magnetoelectric effect in noncollinear magnets. *Phys Rev Lett* 95:057205.
- [16] Chapon LC et al. (2004) Structural anomalies and multiferroic behavior in magnetically frustrated TbMn_2O_5 . *Phys Rev Lett* 93:177402.
- [17] Chapon LC et al. (2006) Ferroelectricity induced by acentric spin-density waves in YMn_2O_5 . *Phys Rev Lett* 96:097601.
- [18] Cheong S-W, Mostovoy M (2007) Multiferroics: a magnetic twist for ferroelectricity. *Nat Mater* 6:13-20.
- [19] Blazey KW, Rohrer H, Webster R (1971) Magnetocaloric effects and the angular variation of the magnetic phase diagram of antiferromagnetic GdAlO_3 . *Phys Rev B* 4:2287-2302.
- [20] King AR, Rohrer H (1979) Spin-ops bicritical field in MnF_2 . *Phys Rev B* 19:5864-5876.
- [21] Kanamori J (1963) in Magnetism, eds Rado GT & Suhl H (Academic Press, New York), pp 127-203.
- [22] Koo J et al. (2007) Non-resonant and resonant X-ray scattering studies on multiferroic TbMn_2O_5 . *Phys Rev Lett* 99:197601.
- [23] Haam SY et al. (2006) Evolution of ferroelectric and antiferromagnetic phases of TbMn_2O_5 under high magnetic field up to 45 T. *Ferroelectrics* 336:153-159.
- [24] Strykowski E, Giordano N (1977) Metamagnetism. *Adv Phys* 26:487-650.
- [25] Khmel'nitskii DE, Shneerson VL (1971) Low-temperature displacement-type phase transition in crystals. *Sov Phys Solid State* 13:687-694.
- [26] Kvyatkovskii OE (2001) Quantum effects in incipient and low-temperature ferroelectrics (a review). *Phys Solid State* 43:1401-1419.
- [27] Wang R, Sakamoto N, Itho M (2000) Effects of pressure on the dielectric properties of $\text{SrTi}^{18}\text{O}_3$ and $\text{SrTi}^{16}\text{O}_3$ single crystals. *Phys Rev B* 62:R3577-R3580.
- [28] Horiuchi S, Okimoto Y, Kumai R, Tokura Y (2003) Quantum phase transition in organic charge-transfer complexes. *Science* 299:229-232.
- [29] Barrett JH (1952) Dielectric constant in perovskite type crystals. *Phys Rev* 86:118-120.